ELSEVIER

Journal of Fluids and Structures 24 (2008) 281–293

JOURNAL OF FLUIDS AND STRUCTURES

www.elsevier.com/locate/jfs

Influence of nozzle geometry on the near-field structure of a highly underexpanded sonic jet

Y. Otobe[a,*], H. Kashimura[a], S. Matsuo[b], T. Setoguchi[b], H.-D. Kim[c]

[a]*Kitakyushu National College of Technology, Kitakyushu 802-0985, Japan*
[b]*Saga University, Saga 840-8502, Japan*
[c]*Andong National University, Andong, Korea*

Received 29 July 2006; accepted 1 July 2007
Available online 21 September 2007

Abstract

Detailed near-field structures of highly underexpanded sonic free jets have been investigated with the help of computational fluid dynamics. Two-dimensional, axisymmetric Euler equations have been chosen to predict the underexpanded jets, and the third-order total variation diminishing finite-difference scheme has been applied to solve the system of governing equations numerically. Several different nozzles have been employed to investigate the influence of the nozzle geometry on the near-field structures of highly underexpanded sonic free jets. The results obtained show that the distance from the nozzle exit to the Mach disk is an increasing function of the jet–pressure ratio, which also significantly influences the shape of the jet boundary. The diameter of the Mach disk increases with the jet–pressure ratio, and it is further significantly influenced by the nozzle geometry, unlike the distance of the Mach disk from the nozzle exit. However, such a dependence on the nozzle geometry is no longer found when an effective-diameter concept is taken into account for the flow from a sharp-edged orifice. A good correlation in the diameters of the Mach disk is obtained, so that the near-field structure of highly underexpanded sonic free jets is a unique function of the pressure ratio, regardless of the nozzle geometry.

Keywords: Compressible flow; Axisymmetric flow; Nozzle; Sonic jet; Mach disk; Vena contracta

1. Introduction

An underexpanded free jet is one of the simplest flows and has a number of practical applications ranging from the design of rocket-propulsion systems to industrial areas using high-pressure gases. A great deal of work has been done to investigate the major features of sonic free jets (Chuech et al., 1989; Meier et al., 1990; Birkby and Page, 2001). According to these studies, the flow pattern of a jet issuing from a nozzle or an orifice depends primarily on the ratio of the nozzle exit pressure to the ambient pressure. Depending on this pressure ratio, three patterns of jets are possible: subsonic, moderately underexpanded and highly underexpanded. The values of the pressure ratio separating these three flow patterns are dependent on the specific heats of the gases, although the variation from one gas to another is quite small (Driftmyer, 1972; Palmer and Hanson, 1998).

In subsonic free jets, the nozzle exit pressure always matches the ambient pressure, while in underexpanded jets, the nozzle exit pressure is higher than the ambient pressure. With an increase in the nozzle exit-to-ambient pressure ratio,

*Corresponding author. Tel./fax: +81 93 964 7298.
E-mail address: otobe@kct.ac.jp (Y. Otobe).

0889-9746/$ - see front matter
doi:10.1016/j.jfluidstructs.2007.07.003

Nomenclature

C_d	discharge coefficient
D	diameter of Mach disk or diameter of nozzle exit
e	internal energy per unit volume
L	distance from nozzle exit to Mach disk
M	Mach number
p	pressure
R	radius of curvature of nozzle or gas constant
r	radial distance
S	entropy
u	axial velocity
v	radial velocity
x	axial distance
β	convergence angle of sharp-edged orifice (deg)
θ	local angle of jet boundary (deg)
κ	ratio of specific heats
ρ	density

Super/Subscripts

b	ambient state
B	jet boundary
e	nozzle exit
m	Mach disk
o	total state

the sonic jet changes from moderately underexpanded to highly underexpanded. These two jets are mostly distinguished by the appearance of a Mach disk inside the jet (Adamson and Nicholls, 1959; Ashkenas and Sherman, 1966; Powell, 1988). In general, the degree of underexpansion of the jet affects the entrainment of ambient gas into the jet, as well as the fundamental flow structure inside the jet. Moreover, the Mach disk is of practical importance in industrial applications using jet-impingement technology, since it directly influences the impact pressures or loads that are very frequently subject to strong variations.

Many studies have shown that the Mach disk is one of the most important factors specifying highly underexpanded sonic jets. Billig et al. (1971), Saito et al. (1986) and Narayanan and Damodaran (1993) have investigated the diameter of the Mach disk, the distance from the nozzle exit to the Mach disk and the configuration of the jet boundary. They have argued that all these are functions of the pressure ratio only. Using several different nozzles Addy (1981) has shown that the nozzle geometry does not affect the distance of the Mach disk, but he has pointed out that the geometry has some influence on the diameter of the Mach disk. Many other researchers have reported the same results as Addy (1981) [see, for example, Lengrand et al., 1982; Cumber et al., 1995]. Thus, some conflict exists with regard to the effect of the nozzle geometry on the underexpanded jet structure. However, no acceptable explanation of this problem has been given to date.

Cumber et al. (1995) have collected the experimental data of many other researchers and showed that the distance of the Mach disk from the nozzle exit correlates quite well with the pressure ratio, but the correlation of the diameters of the Mach disk is relatively poor. However, they did not give any reason for this poor correlation, but vaguely inferred that it could result from the different nozzles used in each experiment. More study is therefore required to investigate how the nozzle geometry influences the Mach disk and to find out the reasons for the poor correlation of the diameter of the Mach disk with the pressure ratio.

In general, it is believed that the Mach disk is generated by reflection of the barrel shock waves that are formed near the highly underexpanded jet boundary (Abbett, 1971; Fox, 1974). Therefore, the shape of the Mach disk would be influenced by the curvature of the barrel shock wave, which, in turn, is closely related to the detailed expansion processes of gases. For instance, the expansion of gases through an orifice with a sharp edge can be somewhat different from that through a straight nozzle. The Vena contracta (flow contraction) phenomenon almost always appears in flows through a sharp-edged orifice, while it seldom occurs in straight nozzles.

In the present study, computational fluid dynamics has been applied to clarify the near-field structure of highly underexpanded sonic free jets. Several different nozzles have been employed to investigate the influence of the nozzle geometry on the Mach disk. Based upon the present computational results, the concept of an imaginary straight nozzle that takes account of the flow-contraction effect was introduced to the flow through an orifice with sharp edges. It was then found that the near-field structure of highly underexpanded sonic free jets is a unique function of the pressure ratio, regardless of the nozzle geometry. Using the proposed concept, a good correlation in the diameter of the Mach disk was obtained, regardless of the nozzle geometry.

2. Computational method and boundary conditions

In the near-field of highly underexpanded sonic free jets, it is assumed that the flow structure is not significantly influenced by viscous effects. Consequently, the unsteady, axisymmetric form of the inviscid flow equations has been

chosen in the present study and it is given by Eq. (1) in the cylindrical coordinate system (x,r):

$$\frac{\partial \mathbf{U}}{\partial t}+\frac{\partial \mathbf{F}}{\partial x}+\frac{\partial \mathbf{G}}{\partial r}+\mathbf{H}=\mathbf{0}, \tag{1}$$

$$\mathbf{U}=\begin{pmatrix}\rho\\ \rho u\\ \rho v\\ e\end{pmatrix},\quad \mathbf{F}=\begin{pmatrix}\rho u\\ \rho u^2+p\\ \rho uv\\ (e+p)u\end{pmatrix},\quad \mathbf{G}=\begin{pmatrix}\rho v\\ \rho uv\\ \rho v^2+p\\ (e+p)v\end{pmatrix},\quad \mathbf{H}=\frac{1}{r}\begin{pmatrix}\rho v\\ \rho uv\\ \rho v^2\\ (e+p)v\end{pmatrix}.$$

The internal energy per unit volume e is given by Eq. (2) in terms of the ratio $\kappa(=1.4)$ of specific heats and pressure p:

$$e=\frac{p}{\kappa-1}+\frac{\rho}{2}\left(u^2+v^2\right). \tag{2}$$

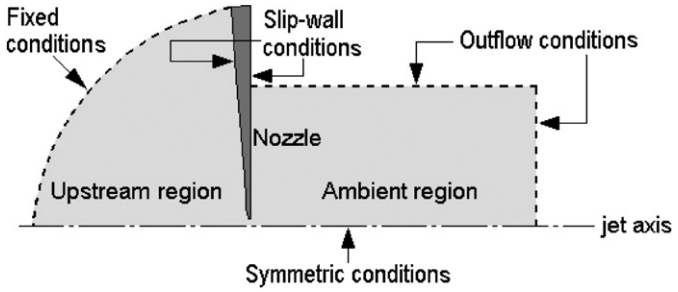

Fig. 1. Computational domain and boundary conditions.

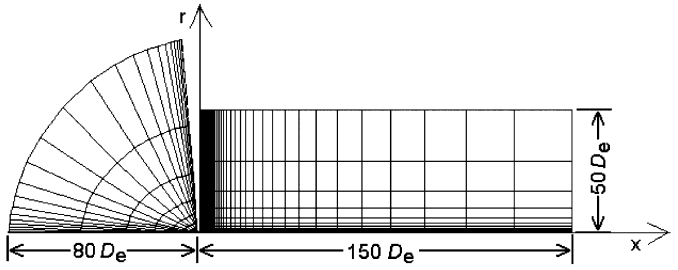

Fig. 2. Computational grid system (D_e: diameter at nozzle exit).

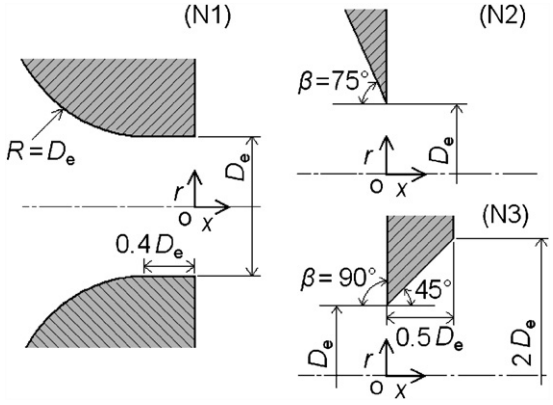

Fig. 3. Nozzle geometries used in the present study.

Eq. (1) is converted into a computational plane ($\xi-\eta$), using the general transformation technique with the components of contravariant velocity,

$$U = \xi_x u + \xi_r v, \quad V = \eta_x u + \eta_r v, \tag{3}$$

where the Jacobian determinant J is given by

$$J = x_\xi r_\eta - x_\eta r_\xi. \tag{4}$$

Solutions were obtained by integrating the time-dependent form of the above equations numerically to a steady state. The integration of the equations was performed using the third-order accurate TVD (total variation diminishing) finite-difference scheme (Yee, 1989). This scheme makes it feasible to capture the shock structure in the highly underexpanded sonic jets, but only with fine computational grids in the vicinity of the shock waves and jet boundaries.

In all the computations, a symmetric boundary was imposed along the jet axis. Fixed-pressure boundary conditions were applied to the upstream boundary of the computational domain and outflow conditions to the downstream boundary, respectively. Along the nozzle walls, adiabatic slip boundary conditions were assumed (see Fig. 1).

The fineness of the computational grid required to obtain grid-independent solutions was examined for each of the jets studied. Fig. 2 shows the typical numerical grid system employed in the present study. The computational region is extended to $80D_e$ upstream of the nozzle, where D_e is the diameter of the nozzle exit. Meanwhile, the computational region downstream of the nozzle is extended to $150D_e$ and $50D_e$, in the axial and radial directions, respectively. The computational grids are clustered to obtain reasonable solutions in the flow regions with a large gradient in pressure and velocity. Several preliminary tests on different computational grids have been performed to obtain grid-independent solutions. The resulting numbers of computational grids applied are 35×30 in the region upstream of the nozzle, and 200×60 in the region downstream of the nozzle.

In the present study, the nozzle supply-to-ambient pressure ratio p_o/p_b was varied in the range between 4.0 and 12.0, corresponding to a nozzle exit-to-ambient pressure ratio in the range 2.11 to 6.34. The working gas was assumed to be air at room temperature.

3. Nozzle geometries

Addy (1981) carried out several experiments using different nozzle geometries to investigate the effects of this on the Mach disk of highly underexpanded sonic free jets. In the present study, the three types of nozzles previously employed in Addy's work have been adopted, as shown schematically in Fig. 3. N1 is a cylindrical straight nozzle of exit diameter D_e and radius of curvature $R = D_e$ at the entrance. A straight section of length $0.4D_e$ is followed by a convergent section. N2 and N3 are sharp-edged orifices with geometrically the same diameter as that of the straight nozzle. N2 has a convergence angle $\beta = 75^\circ$ at the entrance, while N3 has $\beta = 90^\circ$, but the orifice exit diverges with 45° over the length $0.5D_e$.

4. Results and discussion

4.1. Predicted iso-density contours and stream lines

Fig. 4 shows a comparison of the present computational results with the experimental ones (Otobe et al., 2006). The shadowgraph visualization is shown in the lower half, while the present computational results are given as predicted iso-density contours in the upper half. The flow is underexpanded at the nozzle exit, barrel shock waves are formed due to the pressure difference between the underexpanded gas and the ambient gas, and these shock waves reflect from the jet axis, consequently leading to a Mach disk near the jet axis. A triple point is formed at the intersection of the Mach disk with the barrel shock wave. A slipstream is observed downstream of the triple point. The predicted iso-density contour is nearly the same as the flow visualization result. In more detail, the present computations predict the diameter and the distance of the Mach disk to be $D_m/D_e = 0.43$ and $L_m/D_e = 1.58$, respectively, while the experimental values are 0.43 and 1.57, respectively. Thus, the present computations predict well the near-field structure of the highly underexpanded sonic jets.

For pressure ratios of 7.0, 9.0 and 12.0, Fig. 5 shows the predicted entropy difference normalized by the gas constant R, where S is the local value of the entropy and S_o is the entropy under upstream stagnation conditions. The entropy is constant from the nozzle exit to the Mach disk, where it sharply increases up to a certain level corresponding to the strength of the Mach disk. The present computational algorithm predicts well the isentropic character of the flow in the jet core.

Typical results of the near-field structures of highly underexpanded jets issuing from the straight nozzle N1 and the sharp-edged orifice N2 are presented in Fig. 6, where the pressure ratio p_o/p_b is 8.0. The predicted iso-density contours are shown in the upper half of Fig. 6, while the streamlines are shown in the lower half. The detailed near-field structures, such as the barrel shock waves, the Mach disk and the jet boundary, are known from the iso-density contours, while the expansion processes of the gas are observed in the predicted streamlines. Some major differences in both jets are found in the jet boundary, the barrel shock wave and the diameter of the Mach disk. These are due to the flow-contraction effect that occurs at the exit of the sharp-edged orifice.

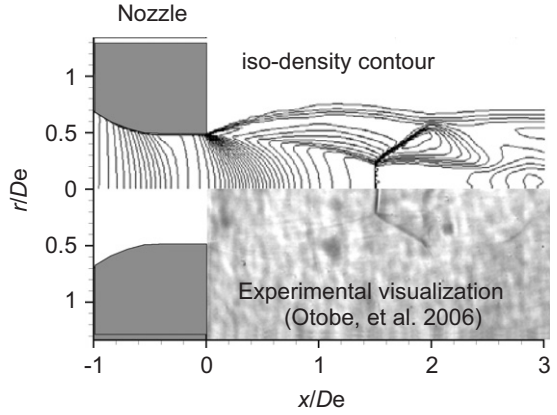

Fig. 4. Comparison of the present computation with experiment (Nl and $p_o/p_b = 6.2$).

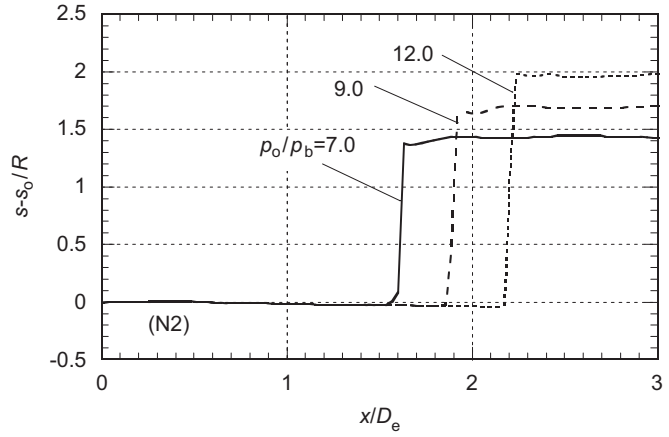

Fig. 5. Entropy variations along the jet axis (N2).

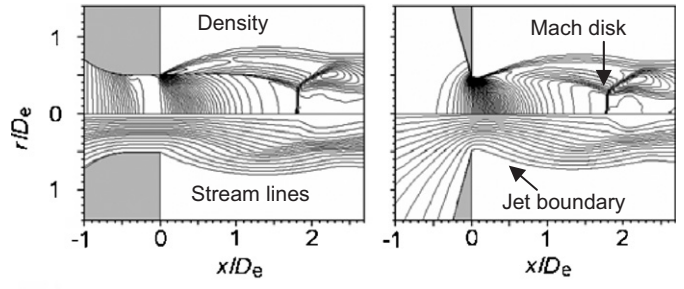

(a) **N1** (b) **N2**

Fig. 6. Comparison of underexpanded jet structures issuing from two different nozzles ($p_o/p_b = 8.0$).

4.2. Diameter and distance of Mach disk

The correlation between the diameter D_m/D_e of the Mach disk and the pressure ratio p_o/p_b is shown in Fig. 7, where the present computational results are again compared with the results of Addy's experiments. For the three geometries used, the diameter of the Mach disk is an increasing function of the pressure ratio, and the present computations predict the diameter of the Mach disk with quite good accuracy. It is interesting to note that this diameter is significantly influenced by the nozzle geometry; for a given pressure ratio, the diameter of the Mach disk for the straight nozzle is appreciably larger than those for the other two orifices.

It seems that the critical pressure ratio (shown by $(p_o/p_b)_c$ in the figure) for the Mach disk to begin to form is also dependent on the nozzle geometry, the critical pressure ratio for the straight nozzle being somewhat lower than those for the sharp-edged orifices. As shown in Fig. 6, it is believed that the streamline curvature in the straight nozzle is different from those in the orifices.

Fig. 8 shows the correlation between the distance from the nozzle exit to the Mach disk and the pressure ratio. It is found that the distance L_m of the Mach disk is given by a function of the pressure ratio and it is not sensitive to the nozzle geometry, unlike the diameter of the Mach disk. This fact can also be confirmed from the predicted static-pressure distributions in Fig. 9, where $x/D_e = 0$ means the nozzle exit. The static-pressure distributions upstream of the nozzle exit are strongly dependent on the nozzle geometry, but downstream of the nozzle, they are nearly the same for

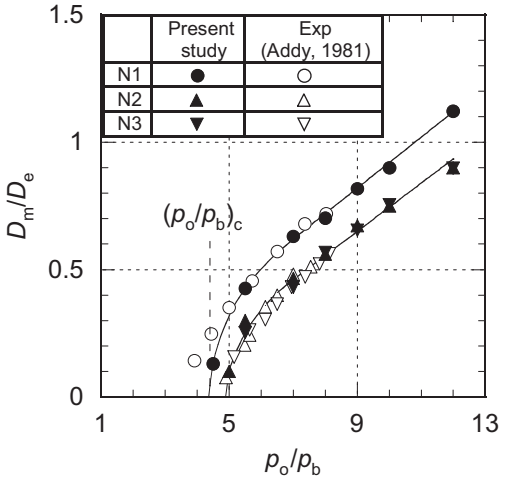

Fig. 7. Correlation between p_o/p_b and diameter of Mach disk.

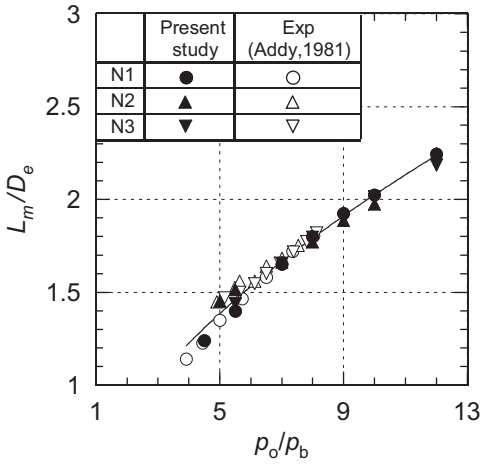

Fig. 8. Correlation between p_o/p_b and distance of Mach disk.

the three different nozzles. The location of the sharp jump in the static-pressure distribution is the same, regardless of the nozzle geometry. The present data obviously show that the distance of the Mach disk from the nozzle exit can be predicted by the pressure ratio alone, regardless of the nozzle configuration.

4.3. Vena contracta and corrected diameter of nozzle

A comparison of the boundaries of highly underexpanded sonic jets is shown in Fig. 10, where the thick solid line is the present computational result, and the thin solid line was obtained by Adamson and Nicholls (1959) using the method of characteristics. Note that the present jet boundary is defined using a limiting streamline (the outermost streamline) of the jet. The location denoted as 'T' is the triple point of the shock waves obtained by the present study. From many examples of flow visualizations of highly underexpanded sonic jets, which have been performed by many researchers [see, for example, Wlezien, 1989; Yu et al., 1998; Venkatakrishanan, 2005], it is known that the jet boundary has a cell structure, being convex a little upstream of the Mach disk. The present computational results predict such a jet-boundary shape, which is quite similar to the theoretical line obtained by the method of characteristics.

Fig. 11 shows the effect of the pressure ratio on the predicted configuration of the jet boundary. It is found that the pressure ratio is obviously a key parameter in determining the jet boundary; as the pressure ratio is increased, the jet boundary expands. This trend is the same for the three nozzles. However, it is worth noting that the gas flow through the orifices has the Vena contracta just downstream of the orifice exit (Fig. 11(b) and (c)), while the flow-contraction effect does not occur in the straight nozzle (Fig. 11(a)), as expected. The present results imply that the nozzle geometry should have some influence on the near-field structure of highly underexpanded sonic jets.

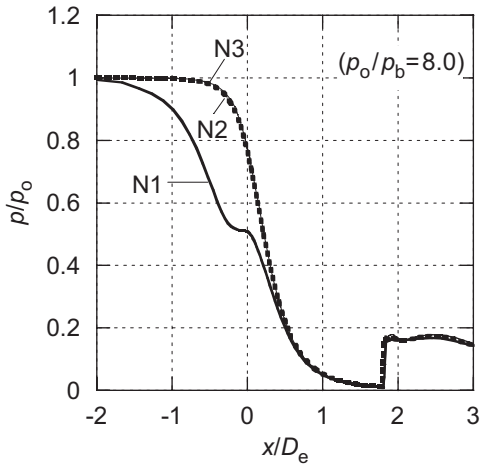

Fig. 9. Comparison of static pressure distributions along the jet axis for the three types of nozzles ($p_o/p_b = 8.0$).

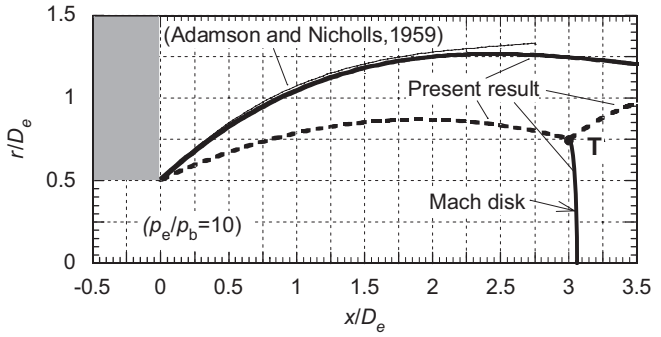

Fig. 10. Comparison of jet-boundary configurations ($p_e/p_b = 10.0$).

In order to investigate quantitatively the vena contracta effect that appears in the orifices, their coefficients of discharge C_d (Munson et al., 1990) are plotted in Fig. 12. The coefficient of discharge is essentially 1.0 for the straight nozzle, but for the two orifices it is expressed by a weak function of the convergence angle β. It is known from the present computations that the coefficient of discharge is 0.85 for $\beta = 75^\circ$ and 0.83 for $\beta = 90^\circ$. This value of 0.83 is exactly the same as the value reported by Liepmann (1961). It also seems that the present data are not greatly influenced by the applied pressure ratios. Note that this value of the coefficient of discharge does not arise from viscous effects near the wall surfaces, but from the streamline curvature effect at the orifice exit, since viscous effects were not considered in the present computations.

In order to investigate the vena contracta effect on the near-field of the jet in more detail, Fig. 13 shows a schematic diagram of the near-field of a highly under expanded sonic jet issuing from a sharp-edged orifice. The flow structure was recast based upon the present computational results. The location 'e' is the geometrical exit of the sharp-edged orifice, 'v' is the vena contracta, where the flow passage has the minimum cross-sectional area, and 'k' is the kink point of the

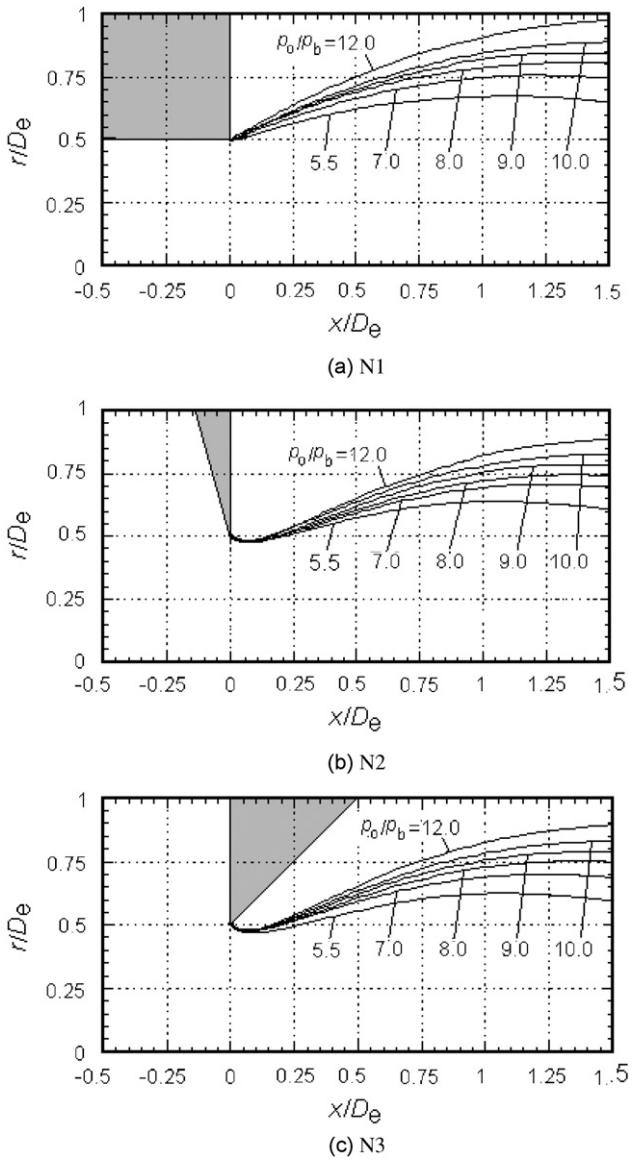

Fig. 11. Variation of jet boundary with pressure ratio.

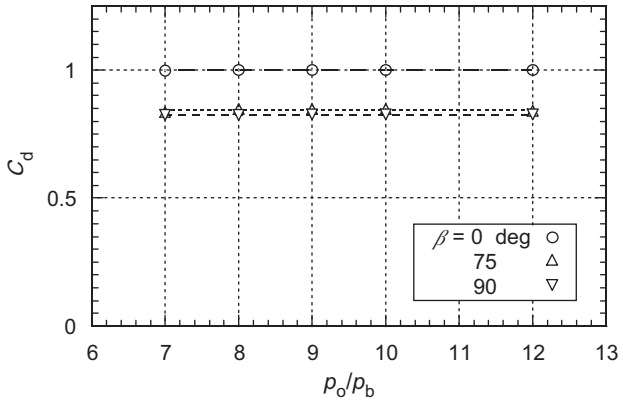

Fig. 12. Correlation between p_o/p_b and discharge coefficient.

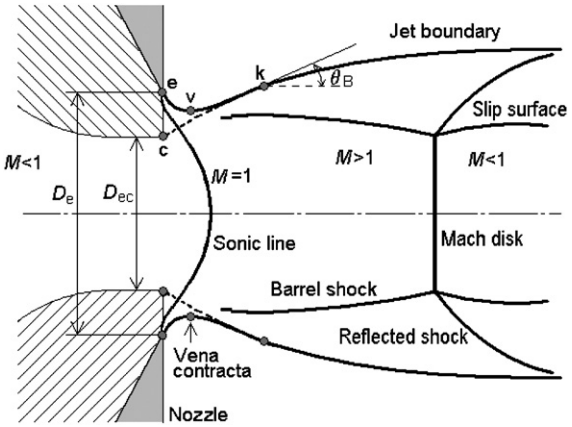

Fig. 13. Schematic illustration showing vena contracta and an imaginary straight nozzle equivalent to an orifice with a sharp edge.

jet boundary. Thus, it is assumed that the outmost streamline follows the line connecting the points 'e', 'v' and 'k'. 'c' is obtained by the intersection point between the vertical line extending from the orifice exit and the tangential line at the kink point. By doing this, we obtain an effective straight nozzle with diameter D_{ec} that is equivalent to an orifice with diameter D_e. In other words, D_{ec} is the exit diameter of an imaginary straight nozzle corresponding to a sharp-edged orifice of diameter D_e.

Meanwhile, the barrel shock waves are generated at the exit of nozzle and then these shock waves experience the Mach reflection on the jet axis, leading to the Mach disk and the reflected shock wave. A triple point is formed due to the intersection of the three shock waves. From this point, the slip stream is generated by the velocity difference between the flows past the two oblique shock waves and the Mach disk. The flow is supersonic upstream of the Mach disk and it becomes subsonic downstream of it.

Fig. 14 shows the correlation between D_{ec}/D_e and p_o/p_b for the three geometries. D_{ec} is identical to D_e in the straight nozzle, but in the two orifices, D_{ec}/D_e is constant at about 0.8, regardless of p_o/p_b. This difference in D_{ec}/D_e value is due to the vena contracta that occurs in the orifices. Fig. 15 shows the correlation between the pressure ratio and the diameter D_m of the Mach disk normalized by D_{ec}. The large scatter in the data previously observed by other workers (Billig et al., 1971; Addy, 1981; Cumber et al., 1995) is no longer found, and there is no appreciable dependence of the diameter of the Mach disk on the nozzle geometry. Therefore, it can be concluded that the scattering in the correlation data for the diameter of the Mach disk is not attributable to the difference in the nozzle diameters employed, but to the difference in shape of the convergent section of the nozzles.

From the present correlation data, D_m/D_{ec} is a linear function of the pressure ratio, regardless of the nozzle geometry:

$$D_m/D_{ec} = 0.115 p_o/p_b - 0.25. \tag{5}$$

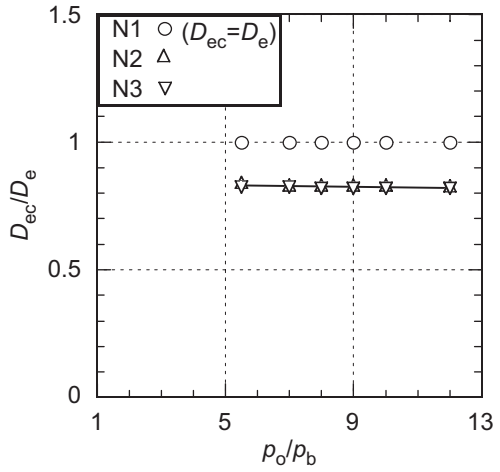

Fig. 14. Correlation between p_o/p_b and D_{ec}/D_e.

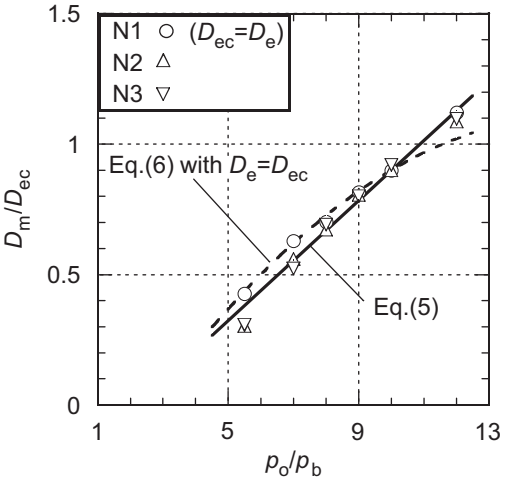

Fig. 15. Correlation between p_o/p_b and D_m/D_{ec}.

In Fig. 15, Eq. (5) is indicated by the solid line, and for the purpose of comparison, Addy's empirical equation, which is approximated by

$$D_m/D_{ec} = 0.36(p_o/p_b - 3.9)^{1/2}, \tag{6}$$

is also given by the dotted line.

Therefore, from Eq. (5) we can predict the diameter of the Mach disk as a function of the pressure ratio alone, provided that the effective nozzle diameter is used to investigate the major characteristics of under expanded jets.

4.4. Jet boundary and Mach disk diameter

Meanwhile, the geometry of the jet boundary at the near-field is closely related to the process of expansion of a gas through a nozzle. This is also associated with the way the Mach disk is generated in highly underexpanded jets. In order to investigate the jet boundary geometry at near-field, the local angle of the jet boundary is defined as θ_B, as indicated in Fig. 13.

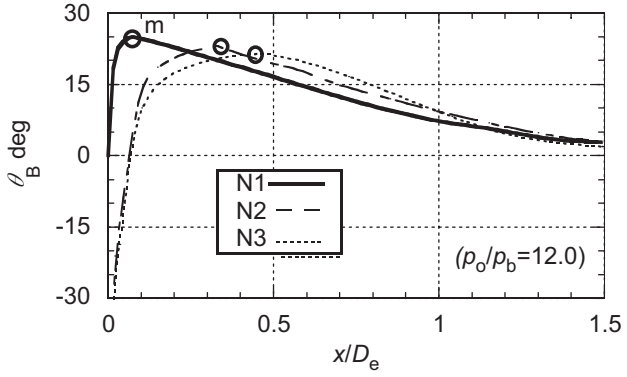

Fig. 16. Variation of θ_B with distance ($p_o/p_b = 12.0$).

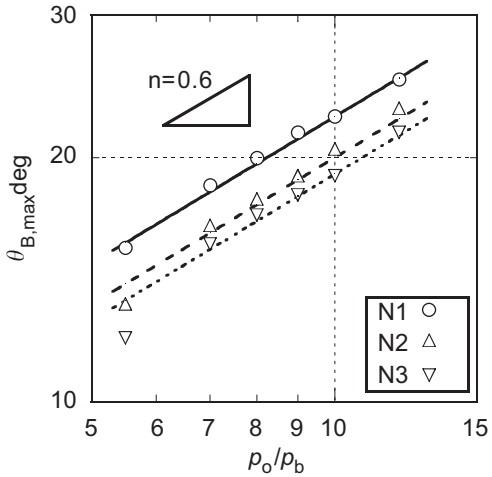

Fig. 17. Correlation between p_o/p_b and θ_B,max.

For the three geometries, Fig. 16 shows the variation in θ_B with the distance x/D_e. Due to the presence of the vena contracta in the orifices, θ_B has a negative value just downstream of the orifice exit, but for all of the three geometries, it sharply increases with distance, and has a peak value (denoted by 'm'), that is dependent on the nozzle geometry and the pressure ratio. After reaching this peak value, it then gradually decreases with distance. It is known that for a given pressure ratio, the peak value of θ_B is largest in the straight nozzle. This indicates that at a given pressure ratio, the jet is more expanded in the straight nozzle than in the orifices. In the range of x/D_e larger than 1.0, it seems that θ_B is essentially the same, regardless of the nozzle geometries employed. Thus, the present results are limited to the near-field of the under-expanded jet.

Fig. 17 shows the correlation between the peak value of θ_B ($= \theta_{B,\max}$) and the pressure ratio for the three geometries. For a given pressure ratio, the peak value $\theta_{B,\max}$ is largest in the straight nozzle, but it is nearly the same in the two orifice nozzles. In more detail, when the pressure ratio is given by 8.0, $\theta_{B,\max}$ is about 20° for N1, being larger than the value for N2 and N3. In the range of pressure ratios applied in the present study, the peak value $\theta_{B,\max}$ linearly increases with the pressure ratio. The slope n in it to the pressure ratio seems to be the same for the three different nozzles. Thus, the peak value $\theta_{B,\max}$ can be given as an empirical equation,

$$\theta_{B,\max} = C(p_o/p_b)^{0.6}, \tag{7}$$

where C is a constant depending on the nozzle geometry. Fig. 18 shows the variation of C with the convergence angle β of the orifices. It seems that the value of C is a decreasing function of the convergence angle β. For the straight nozzle ($\beta = 0$), it is 5.65, but it decreases when β increases. The present C value is applicable to the range of the pressure ratio

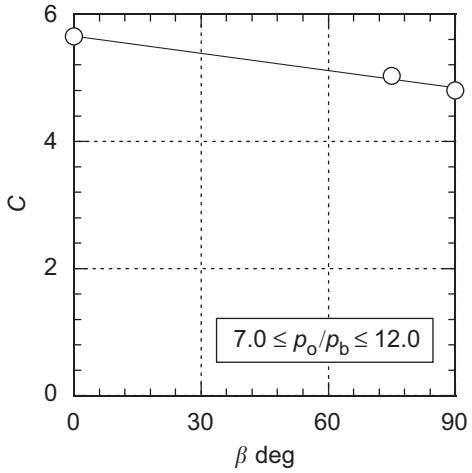

Fig. 18. Variation of C with β.

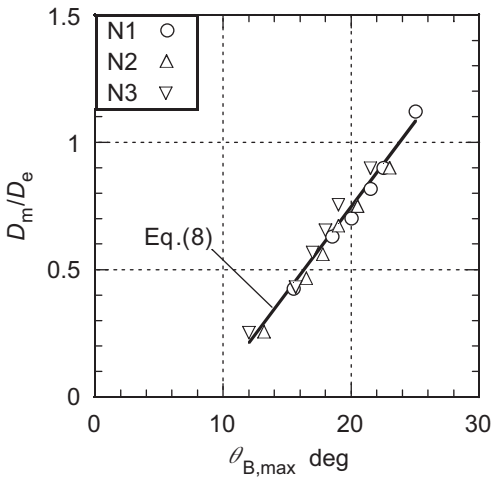

Fig. 19. Correlation between $\theta_{B,\max}$ and D_m/D_e.

of $7.0 \leq p_o/p_b \leq 12.0$, which belongs to the range of moderately under expanded to strongly under expanded jets for the convergent nozzles.

Fig. 19 shows the correlation of the diameter of the Mach disk with the peak value $\theta_{B,\max}$. A good correlation is obtained regardless of the nozzle geometry. It is found that the diameter of the Mach disk is a linear function of the peak value $\theta_{B,\max}$, as given by the empirical equation

$$D_m/D_e = 0.067\theta_{B,\max} - 0.59. \tag{8}$$

From both Eq. (7) and (8), it is known that the increase in the diameter of the Mach disk with the pressure ratio is due to the increase in the peak value $\theta_{B,\max}$. This indicates that the variation in the Mach disk diameter with the pressure ratio is due to detailed expansion process of the jet at the exit of nozzle. According to some empirical equations obtained in the present study, we can obtain the major structure of the jet without the need for an experiment, which is very meaningful and useful in practical engineering applications for predicting the distance and diameter of the Mach disk in under expanded jets.

5. Conclusions

A computational method has been applied to investigate the near-field structure of highly underexpanded sonic free jets. Three different nozzle geometries have been employed to investigate the influence of the nozzle geometry on the near-field structure. Based upon the present computational results, the concept of an imaginary straight nozzle was introduced to take account of the flow contraction effect for sharp-edged orifice nozzles. The present study has led to several important conclusions regarding the influence of the nozzle geometry on the near-field structure of highly underexpanded sonic free jets, which was not well understood in the past.

The distance of the Mach disk from the nozzle exit is a function of the pressure ratio and is not sensitive to the nozzle geometry, unlike the diameter of the Mach disk. For a given nozzle geometry, the geometry of the jet boundary at near-field is also strongly influenced by the pressure ratio. It is found that the diameter of the Mach disk is influenced by both the pressure ratio and the nozzle geometry. However, provided that the concept of an effective diameter is taken into account for the flow from a sharp-edged orifice, the diameter of the Mach disk is independent of the nozzle geometry. Therefore, it can be concluded that the scattering in the correlation data for the diameters of the Mach disk is not attributable to the difference in the nozzle diameters employed, but to the differences in the shape of the convergent section of the nozzles, leading to different flow-contraction effects. Under these circumstances, the diameter of the Mach disk is a linear function of the peak value of the local angle of the jet boundary at near-field. Based upon the present study, some empirical equations have been given to predict the major parameters of underexpanded jets as a function of the pressure ratio.

References

Abbett, M., 1971. Mach disk in underexpanded exhaust plumes. AIAA Journal 9, 512–514.

Adamson, Jr., T.C., Nicholls, J.A., 1959. On the structure of jets from highly underexpanded nozzle into still Air. Journal of Aero/Space Science January, pp. 16–24.

Addy, A.L., 1981. Effects of axisymmetric sonic nozzle geometry on Mach disk characteristics. AIAA Journal 19, 121–122.

Ashkenas, H., Sherman, F.S., 1966. The structure and utilization of supersonic free jets in low density wind tunnels. Rarefied Gas Dynamics 2, 84–105.

Billig, F.S., Orth, R.C., Lasky, M., 1971. A unified analysis of gaseous jet penetration. AIAA Journal 9, 1048–1058.

Birkby, P., Page, G.J., 2001. Numerical predictions of turbulent underexpanded sonic jets using a pressure-based methodology. Journal of Mechanical Engineering 215, 165–173.

Chuech, S.G., Lai, M.C., Faeth, G.M., 1989. Structure of turbulent sonic underexpanded free jets. AIAA Journal 27, 549–559.

Cumber, P.S., Fairweather, M., Falle, S.A.E.G., Giddings, J.R., 1995. Predictions of the structure of turbulent, highly underexpanded jets. ASME Journal of Fluids Engineering 117, 599–604.

Driftmyer, R.T., 1972. A Correlation of freejet data. AIAA Journal 10, 1093–1095.

Fox, J.H., 1974. On the structure of jet plumes. AIAA Journal 12, 105–107.

Lengrand, J.C., Allegre, J., Raffin, M., 1982. Underexpanded free jets and interaction with adjacent surfaces. AIAA Journal 20, 27–28.

Liepmann, H.W., 1961. Gas kinetics and gas dynamics of orifice flow. Journal of Fluid Mechanics 10, 65–79.

Meier, S.G.E.A., Selerowicz, W.C., Szumowski, A.P., 1990. A nozzle generating low jet noise. Journal of Sound and Vibration 136, 65–73.

Munson, B.R., Young, D.F., Okiishi, T.H., 1990. Fundamentals of Fluid Mechanics. Wiley, New York.

Narayanan, A.K., Damodaran, K.A., 1993. Mach disk of dual coaxial axisymmetric Jets. AIAA Journal 31, 1343–1345.

Otobe, Y., Matsuo, S., Tanaka, M., Kashimura, H., Setoguchi, T., 2006. A study on characteristics of under-expanded condensing jet. Transactions of JSME Series B 72, 264–270 (in Japanese).

Palmer, J.L., Hanson, R.K., 1998. Application of method of characteristics to underexpanded, freejet flows with vibrational noneqilibrium. AIAA Journal 36, 193–200.

Powell, A., 1988. The sound-producing oscillations of round underexpanded jets impinging on normal plates. Journal of the Acoustic Society of America 83, 515–533.

Saito, T., Nakatsuji, H., Teshima, K., 1986. Numerical simulation and visualization of freejet flow-fields. Transactions of Japan Society of Aeronautical and Space Sciences 28, 240–247.

Venkatakrishanan, L., 2005. Density measurements in axisymmetric underexpanded jet by background-oriented schlieren technique. AIAA Journal 43, 1574–1579.

Wlezien, R.W., 1989. Nozzle geometry effects on supersonic jet interaction. AIAA Journal 27, 1361–1367.

Yee, H. C., 1989. A class of high-resolution explicit and implicit shock capturing methods. NASA TM-101088.

Yu, Y.K., Chen, R.H., Chew, L., 1998. Screech tone noise and mode switching in supersonic swirling jets. AIAA Journal 1968–1974.